Ultrasonics 133 (2023) 107025

Contents lists available at ScienceDirect

Ultrasonics

journal homepage: www.elsevier.com/locate/ultras

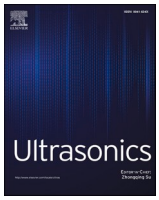

Ultrasonic needle hydrophone calibration in air by a parabolic off-axis mirror focused beam using three-transducer reciprocity

Linas Svilainis [a,*], Andrius Chaziachmetovas [a], Paulius Kaskonas [a], Tomas E. Gomez Alvarez-Arenas [b]

[a] Electronics Engineering Department, Kaunas University of Technology, Kaunas, LT 51368, Lithuania
[b] Ultrasonic and Sensors Technologies Department, Spanish National Research Council (CSIC), Madrid, Spain

ARTICLE INFO

Keywords:
Acoustic metrology
Air-coupled ultrasound
Probe characterization
Plane wave reciprocity
Sensitivity calibration

ABSTRACT

An acoustic field distribution investigation in air requires a small receiving sensor. Needle hydrophones seem to be an attractive solution, and it has previously been demonstrated that needle hydrophones designed for use in water can be used in air. The metrology problem is that an absolute sensitivity calibration is needed, because needle hydrophones are not characterized in air, especially for frequencies below 1 MHz, which is of interest for air-coupled ultrasound. Conventional, three-transducer/microphone reciprocity calibration requires measurements to be done in the far field. However, when transducer diameter is large and the frequency is high, the required measurement distance becomes very large: 3 m for a 20 mm source, transmitting at 1 MHz. Large propagation distance leads to high attenuation and nonlinear effects in air propagation, and distortion and losses accumulate. Small needle hydrophones have low sensitivity, so that high excitation amplitudes would be required, which can lead to transducer heating and increase nonlinearity effects. A derivative of the three-transducer reciprocity calibration method is proposed, where a large aperture transducer is focused onto a hydrophone, using hybrid of plane wave and spherical wave reciprocity. Use of a focused source minimizes the frequency-dependent diffraction effects, and the spherical wave approximation is valid at the focal distance, and low level excitation signals can be used. Focusing is accomplished using a parabolic off-axis mirror. Calibration is in transmission, which reduces the complexity of the electrical measurements. The corresponding equations have been derived for this setup. Calibration of the transducer and needle hydrophone absolute sensitivity is obtained.

1. Introduction

A common task in acoustic metrology, transducer development and quality inspection is the measurement of the acoustic field distribution [1,2]. This task is well documented for high frequencies and water environments [3]. Nevertheless, when it comes to air-coupled ultrasound, the problem becomes complicated. Optical interferometry [4] requires complex and expensive equipment, which is not always available. It is common to use a 3.15 mm diameter microphone (type 4138 microphone from Brüel & Kjær, Nærum, Denmark) [5,6,7,8], but the bandwidth of such microphones is limited to 140 kHz [9]. Furthermore, the size of the sensing element of the receiver, according to [3], should be less than twice the central frequency wavelength of the probe under test, making such a microphone suitable up to 218 kHz, whereas the required size at 1 MHz would be 0.7 mm. Needle hydrophones are intended for immersion use in water, but offer an attractive alternative for use in air, as has been demonstrated previously [10,11]. However, needle hydrophones are not characterized for use in air as calibration is typically done in water for frequencies above 1 MHz, but air-coupled ultrasound is usually below 1 MHz [12].

The three-transducer reciprocity calibration in a free field technique is often used [13,14,15]. The standard [13] for microphones in air recommends a distance between microphones of more than ten nominal diameters. The standard for hydrophones used in water is stricter (see (D.1) on page 62 in [14] for a suitable approximation of spherical wavefront spreading). In the case of air, a 0.5 mm receiver driven by a 20 mm transmitter at 300 kHz should be separated by a distance of 460 mm. If a 20 mm receiver operates with a 20 mm transmitter, the required distance is 917 mm; 3 m is required at 1 MHz for a 20 mm receiver operating with a 20 mm transmitter. Only at such distances is the field uniform over the calibrated probe surface. The influence of reflections from surrounding surfaces increases as the distance between

* Corresponding author.
E-mail address: linas.svilainis@ktu.lt (L. Svilainis).

https://doi.org/10.1016/j.ultras.2023.107025
Received 27 January 2023; Received in revised form 6 April 2023; Accepted 24 April 2023
Available online 4 May 2023

transducers increases, requiring an anechoic chamber, which is burdensome. The fundamental problem with having large propagation distances in air is related to the attenuation and nonlinearity in air [16]: larger propagation distance lead to higher signal distortion and more amplitude loss. Another problem is that the size of the hydrophone is small, and transmission efficiency is low due to a significant transmitter acoustic impedance mismatch with air, leading to a low amplitude received signal. The use of a higher excitation amplitude will not solve this problem, but will make it worse due to non-linearity and transducer heating. Operation at small distances is desirable to make the experimental setup compact. Because of the aforementioned problems, such calibration attempts have previously failed for air [10].

Here we explore an idea, proposed for a substitution calibration of water hydrophones [17]. The use of a focused transmitting transducer minimizes frequency-dependent diffraction effects, so that the spherical wave approximation is valid for small focal distances, and low-level excitation signals can be used. Such an approach results in reduced harmonic generation, which can arise due to nonlinear propagation in air. Use of the focused calibration technique in water is not a new idea [17,18], but there is a problem in applying this to air-coupled ultrasound, due to the lower frequency range. The approach of [17,18] uses a self-reciprocity (reflection from an acoustic, flat mirror) calibration of the transducer. Frequencies, usually used for air-coupled ultrasound, are relatively low, so that tonebursts are long, and signals can overlap when using a pulse-echo configuration, leading to the increased complexity of the electrical measurements. Another problem is that the design of a wideband focusing transducer is complicated, and beam quality is poor. Several matching layers are usually used in the air-coupled transducers to cope with the large acoustic impedance mismatch between the transducer and the air, whilst improving the bandwidth [21]. It is more complicated to manufacture a concave-faced transducer than a flat-faced one, so the solution proposed here is the use of a parabolic, off-axis mirror [19,20]. A wideband, flat-faced, air-coupled transducer [21] is mounted on the off-axis parabolic mirror, to focus the beam onto the needle hydrophone. Then the electrical transfer impedance [13,14] between transducer and hydrophone was measured, assuming spherical wave propagation [17]. Next, the electrical transfer impedance [13,14] was measured between two transducers of the same type, without using focusing. The distance between transducers was the same as was set in the case of focusing, but this time using a plane wave propagation assumption [22]. The through transmission configuration reduces the complexity of the electrical measurements, and the signal overlap problem is reduced. The corresponding equations for the hybrid of plane wave and spherical wave have been derived for such a setup. The sensitivities for both the hydrophone and the flat beam transducers were obtained. Finally, it is complicated to have an extremely broadband transducer if calibration over a broad frequency range is required. It is proposed to use three transducer types with different frequency ranges, and then stitch the results together to obtain an extremely broadband calibration. Applications of the air-coupled transducers are usually in the near field, and therefore the transmission sensitivity in this paper is expressed not as ratio of the sound pressure at a reference distance to the driving current [14], but as the ratio of the sound pressure on the transmitting transducer surface to the driving current. For validation, the calibration of the transducers was also carried out, using a derivative of the substitution technique described in [23], and plane-wave-three-transducers-reciprocity [22]. Validation of the needle hydrophone sensitivity was only possible against the immersion (water) calibration, provided by manufacturer.

2. Equipment and methods

The low sensitivity of the hydrophone is a key challenge, which is due to the small size and acoustic impedance mismatch and the low generation efficiency in air. Large pressures can be achieved in water and the separation distances required are much smaller, meaning that

Fig. 1. Transducers used in experiments (left: 1 MHz, center: 650 kHz, right: 300 kHz center frequency).

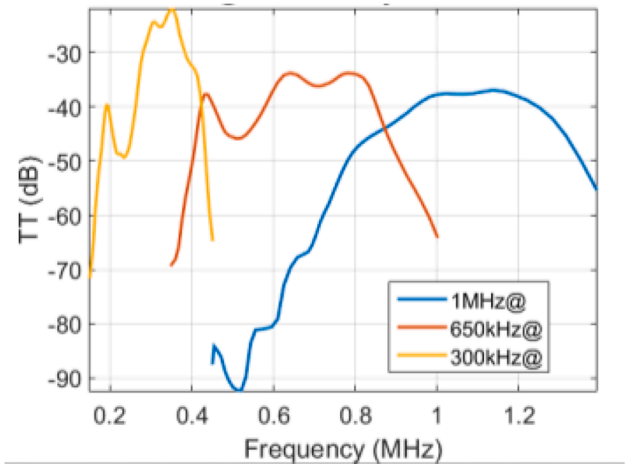

Fig. 2. Transmission frequency response of the transducers used.

three transducer reciprocity, two transducer reciprocity or interferometry are easier to implement [14]. The pressure levels attainable in the air are several orders of magnitude lower, but the nonlinearity appears at much lower pressures for frequencies beyond 100 kHz, and attenuation is much larger. Nonlinearity can be usefully exploited in harmonic calibration, and beam size variation is not as significant as in our case, but a calibrated hydrophone/microphone of the same size is required. A different solution is required, where that are no commercially available microphones and no primary standard of less than 1 mm in size and frequency beyond 100 kHz. These are the reasons for developing the technique described here. The small distance and the large pressure just at single point are the key elements in the proposed approach.

2.1. Transducers and hydrophones used

Large diameter transducers that are extremely well matched to air were used to develop sufficient pressure. Three types of air-coupled transducers (see Fig. 1) with nominal center frequencies of 0.3 MHz 0.65 MHz and 1 MHz and identical encapsulation were used in the experiments. Use of three different frequency ranges facilitated coverage of the broad frequency range required for hydrophone calibration. Three transducers of each type were used, labeled as T_1, T_2 and T_3, i.e. nine transducers in total. T_1 and T_2 were used in the hybrid calibration technique, described in section 2.3. Transducers T_3 were used for validation purposes in three-transducer plane wave reciprocity calibration [22], as described in section 2.5.

The transducers (designed and manufactured by the Spanish National Research Council, CSIC) comprised of a 20 mm diameter piezoelectric disc element, embedded in aluminum case. More details on the transducer design can be found in [21]. The transmission frequency response of these transducers is presented in Fig. 2 (obtained in through transmission (TT) at 25.4 mm distance at 10 Vpp excitation). It can be

Fig. 3. Needle hydrophones used in the experiments (left: 0.5 mm, right: 1 mm).

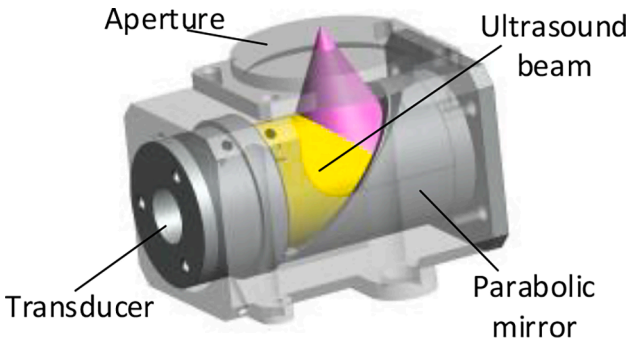

Fig. 4. Holder for parabolic off-axis mirror focusing.

seen that they have a −20 dB bandwidth of 0.2 MHz, 0.54 MHz and 0.66 MHz, for the nominal center frequencies 0.3 MHz, 0.6 MHz and 1 MHz respectively. The range of the passband frequencies of the transducers overlap, so that these three can be used for the calibration of the hydrophone in air over a 0.15–1.4 MHz frequency range.

Two needle hydrophones (see Fig. 3) were used in the investigation: a 0.5 mm diameter sensitive element (NH0500, Precision Acoustics Ltd.) and 1 mm diameter sensitive element (NH1000, Precision Acoustics Ltd.).

The hydrophones have been calibrated in water by the manufacturer, but only over a range of 1–30 MHz. At 1 MHz, the 0.5 mm diameter hydrophone has a sensitivity of 0.777 μV/Pa; while the 1 mm diameter hydrophone has a sensitivity of 1.334 μV/Pa.

2.2. Focusing using parabolic off-axis mirror

The pressure exerted by the transducer, was focused using a parabolic off-axis mirror to increase the SNR at the hydrophone location [20]. In such cases, the spherical wave propagation approximation is valid at the focal point and frequency-dependent diffraction effects are minimized [17]. The use of the parabolic mirrors has been reported previously [19,20,24]. Usually, such an approach is considered problematic because it requires precise mirror production and the mirrors are difficult to align, due to the lack of a well-defined propagation axis. A commercially available, optical grade, off-axis mirror (14OAP-1–25-90-AL type from Standa Photonics) was used, so that the surface quality and manufacturability did not present an issue. The mirror has 90° off-axis focusing at a distance of 25.4 mm and a diameter of 25.4 mm, so that the incoming beam from the transducer with a 20 mm diameter active element is fully covered by the mirror surface. The mirror and the transducer were mounted in a specially designed, 3D printed plastic case (Fig. 4), which minimizes the alignment problems.

An aperture mask (4 mm diameter, 3 mm away before the focal spot, refer Fig. 4) was used to reduce the effect of sidelobes in the beam [11]. The presence of the aperture also solves the beam location issue. Eight screws are used in the holder to fix the transducer, which allows for an easy and quick exchange of the transducers.

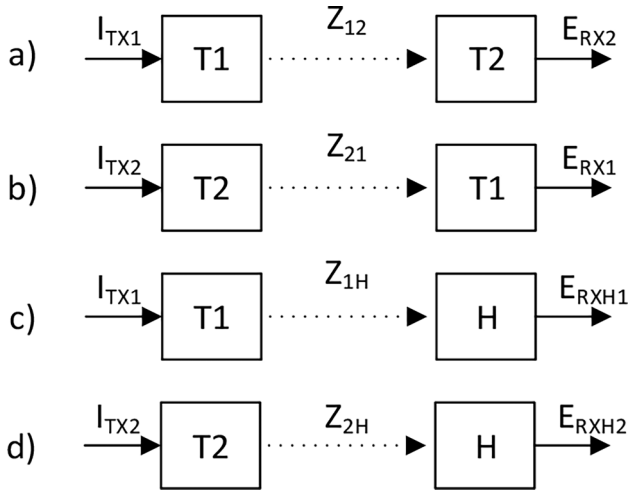

Fig. 5. Three transducers reciprocity calibration setup.

2.3. Three transducers reciprocity calibration using combined plane and focused wave

The large difference in the transducer and the hydrophone size and the different field conditions created another problem: the mathematics required for the sensitivity calculation is missing. The setup involves a focused measurement (transducer-hydrophone), where spherical wave reciprocity applies [17], but there is also another, unfocused measurement (transducer-transducer), where plane wave reciprocity applies. The corresponding equations for the hybrid of plane wave and spherical wave had to be derived for the proposed setup, which would allow one to obtain the sensitivities for both the hydrophone and the flat beam transducers. The three transducers reciprocity calibration was done using three measurements, where at least one transducer used should be reciprocal. The electromechanical reciprocity is [22]:

$$\left|\frac{v}{I_{TX}}\right| = \left|\frac{E_{RX}}{F_0}\right| \tag{1}$$

where v is the velocity of the transmitting surface at a driving current I_{TX}, E_{RX} is the open circuit voltage produced by a force F_0, which is produced by the sound field on a rigid receiving surface. From this, the plane wave reciprocity parameter J_P can be derived [22]:

$$J_P = \left|\frac{M}{S_P}\right| = \frac{2A}{\rho c} S_P = \left|\frac{p_{TX}}{I_{TX}}\right|, M = \left|\frac{E_{RX}}{p_{RX}}\right| A = \pi a^2 \tag{2}$$

where ρ and c are the density and the sound propagation velocity for the coupling media (air was used here), A is the active transducer surface area (obtained using transducer radius a), M is the reception sensitivity, V/Pa, S_P is the transmission sensitivity, expressed as the ratio of the sound pressure on transducer surface p_{TX} to driving current I_{TX}, Pa/A. The input impedance Z_{in} of the amplifier and the transducer impedance Z_T were measured as per [27] and used to convert the voltage registered by the amplifier V_{in} into an open circuit voltage [14]:

$$E_{RX} = \left|\frac{V_{in}\cdot(Z_{in} + Z_T)}{Z_{in}}\right| \tag{3}$$

The hydrophone was used together with a manufacturer-provided preamplifier, with an output impedance of 50 Ω, so that no correction factor was used for these measurements.

The transmission sensitivity can also be expressed in Pa/V, M':

$$M' = M\cdot|Z_T| \tag{4}$$

The electrical transfer impedance is the ratio of the received voltage to the excitation current [13,14]. It was measured in four through-

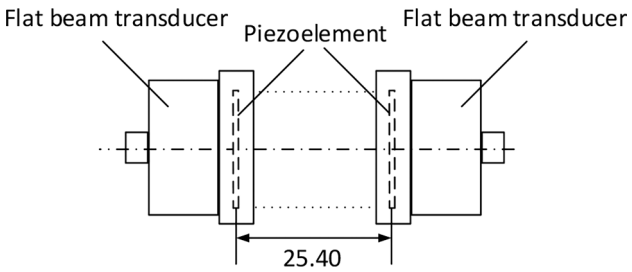

Fig. 6. Near field transducer-transducer transmission measurement setup for plane wave reciprocity measurements.

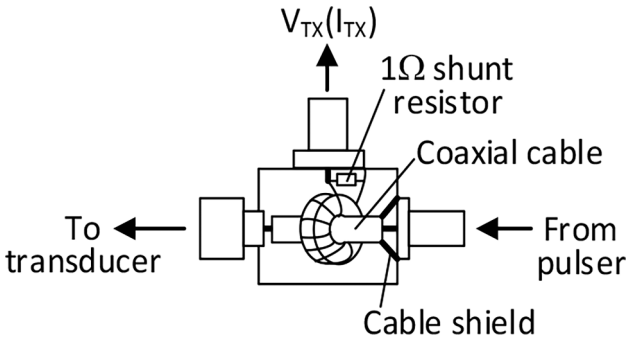

Fig. 7. Design of the current sensor.

transmission configurations (Fig. 5): transducer-transducer (a, b) and transducer-hydrophone (c, d).

The electrical transfer impedance Z_{12} and Z_{21} measured in (a) or (b) configuration was for two of the same types of transducer in the near field (Fig. 6, distance d between transducer elements was 25.4 mm). Measurement (b) is optional and can be omitted: it is an additional measurement used to obtain the hydrophone sensitivity.

The through-transmission configuration reduces the complexity of the electrical measurements, as there is no need for amplifier input protection and the excitation circuit does not affect the received signal. The hydrophone preamplifier output voltage was further amplified by a fixed 40 dB gain, 0.1–3 MHz bandwidth amplifier SE-RX01-02#3 [25] (designed and manufactured at Kaunas University of technology, KTU). A high input impedance (1 MΩ) 0.1–3 MHz bandwidth buffer (0 dB gain) was used for transducer signal reception.

The current of the transmitting transducer was measured simultaneously with the receiving transducer output. The current sensor (Fig. 7) used to measure I_{TX} was made using a miniature N30 ferrite toroidal core (B64290P37X830, EPCOS), mounted on semirigid coaxial cable, connecting the excitation signal path via SMA connectors.

It served as the primary winding of the current transformer, and the secondary winding was made using 10 turns of 0.3 mm diameter, PTFE-coated multicore wire. A 1 Ω shunt resistor was placed in parallel with the secondary winding, which translated into a 10 mΩ shunt in the primary winding. The shield of the cable was connected only to the input connector, coming from the pulser. The same type of amplifier (SE-RX01-02) with 20 dB gain was used to amplify the current signal. A dedicated ultrasonic signal acquisition system [25] was used both to digitize the amplifier output (10 bit analog-to-digit converter (ADC), 100 MHz sampling rate), and to drive the pulser (binary code sets at 100 MHz sampling rate). The transducers were excited by a half bridge topology pulser (SE-TX01-02) [26], using bipolar, +/-5 V rectangular tonebursts (in the 0.15–0.45 MHz range for 300 kHz transducer; in the 0.35–1 MHz range for the 650 kHz transducer; and in the 0.45–1.4 MHz range for the 1 MHz transducer; the total duration was 100 μs). A low excitation voltage was used to avoid transducer heating and distortions. The acquired signals were transferred to a host PC, using a high speed

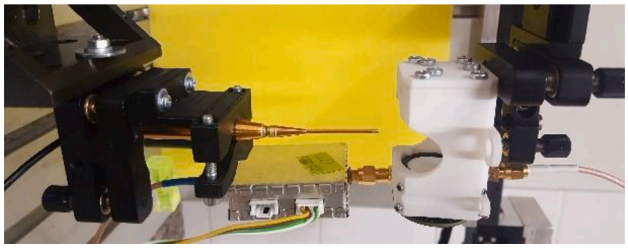

Fig. 8. Transducer holder and hydrophone positioning setup.

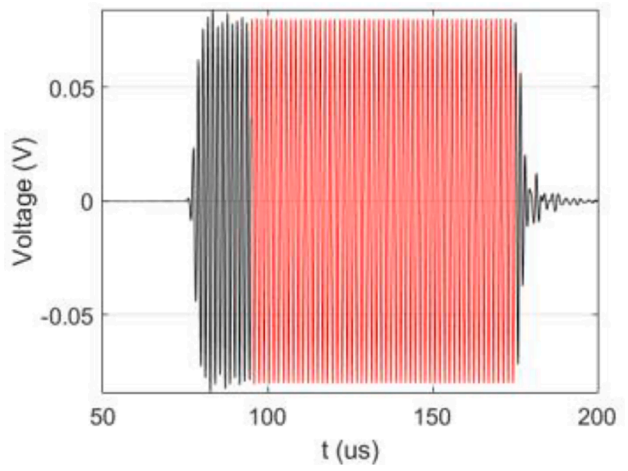

Fig. 9. Toneburst signal registered (black) and SWC result (red) plotted over region used for SWC calculation. (For interpretation of the references to color in this figure legend, the reader is referred to the web version of this article.)

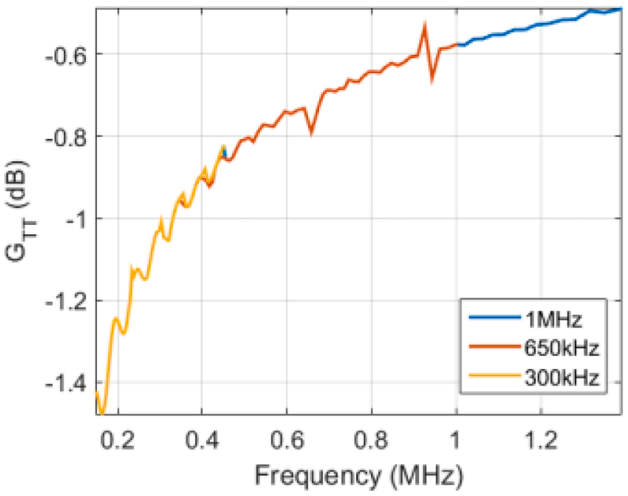

Fig. 10. Diffraction correction for 20 mm piston to 20 mm piston G_{TT} at 25.4 mm distance.

USB 2.0 interface. The tilting of the transducer holder and hydrophone was done using a commercially available kinematic stage (5PM131-2 type from Standa Photonics see Fig. 8). Positioning was done using a computer-controlled 3D positioning system (10 μm resolution for x and y, and 5 μm resolution for z axis) [25].

The amplitude and the phase of the registered current and voltage signals were estimated using the Sine Wave Correlation (SWC) technique [27], using the gated part of the signal (shown in red on Fig. 9).

SWC can be regarded as continuous time Fourier transform at single frequency, or as a lock-in amplifier. Thanks to its narrow bandwidth, it

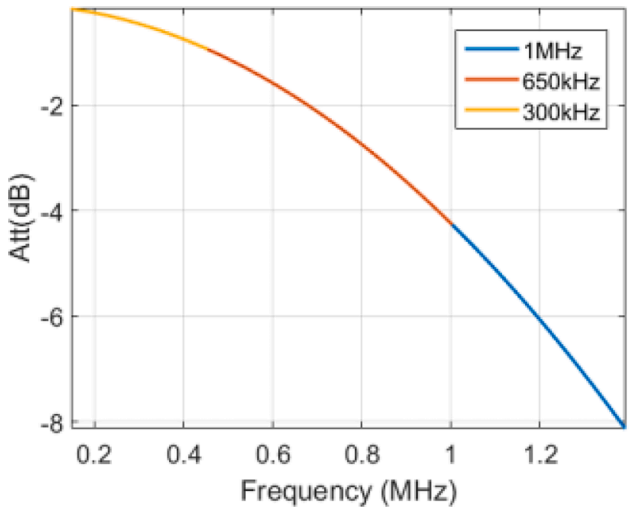

Fig. 11. Attention in air over 25.4 mm distance.

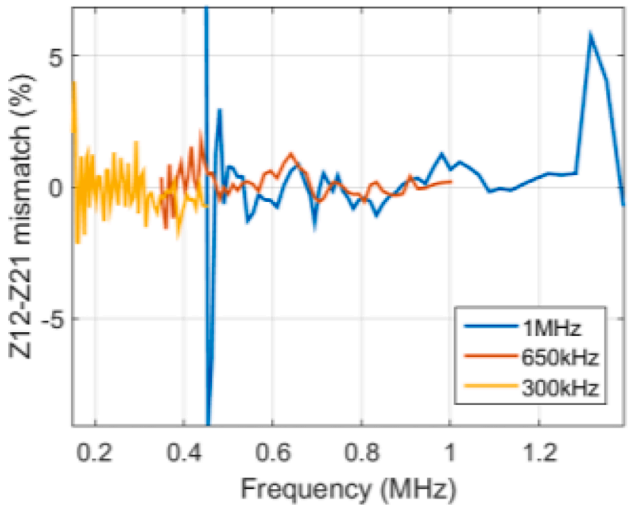

Fig. 12. Reciprocity evaluation as electrical transfer impedance Z_{12} and Z_{21} mismatch (<5% criteria).

can deliver high SNR, and is immune to front ringing caused by the signal's rectangular envelope.

Assuming plane wave propagation [22] and using I_{TX} and E_{RX} derived from (2), the electrical transfer impedance measured in Fig. 5 (a) or (b) configuration can be expressed as:

$$Z_{12} = \frac{E_{RX2}}{I_{TX1}} = S_{P1} M_2 G_{TT} e^{-\alpha d} Z_{21} = \frac{E_{RX1}}{I_{TX2}} = S_{P2} M_1 G_{TT} e^{-\alpha d} \quad (5)$$

where M_2 is the reception sensitivity of transducer T_2, S_{P1} is a plane wave transmission sensitivity for transducer T_1, G_{TT} is the diffraction correction for piston-piston-like wave propagation and the exponential term is the acoustic wave attenuation α (Np/m) in air over a distance d.

The diffraction correction for piston-piston propagation G_{TT} is shown in Fig. 10, with the range applicable to each transducer type indicated by color, and it was calculated using the expression described by (18) in [28], by paraxial expansion.

The attenuation coefficient α (Np/m), can be obtained as described in Annex B in [13]. Attenuation in air over a distance of 25.4 mm is presented in Fig. 11.

Calibration is only possible if transducers T_1 and T_2 are reciprocal. Reciprocity can be evaluated as the electrical transfer impedance Z_{12} and Z_{21} mismatch. According to [14], Z_{12} and Z_{21} should match each other to within 5 %. Fig. 12 is used to present the mismatch for all 3 transducer types used.

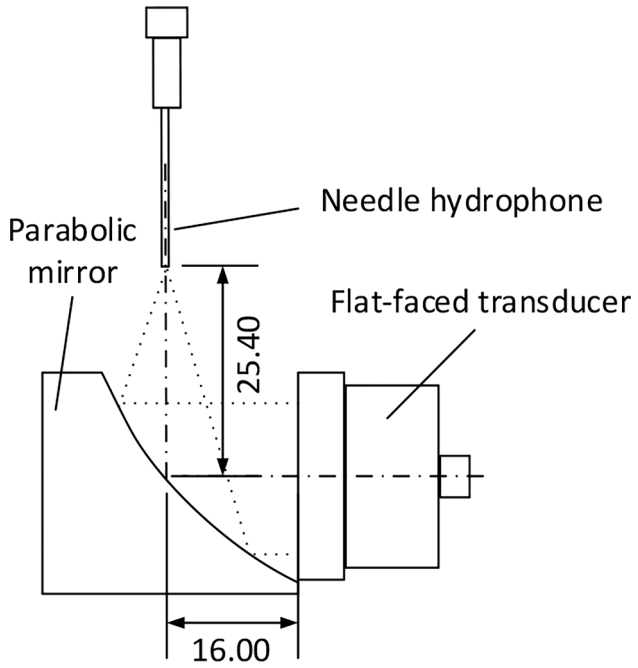

Fig. 13. Focused transducer-hydrophone transmission measurement setup for a spherical wave reciprocity measurements.

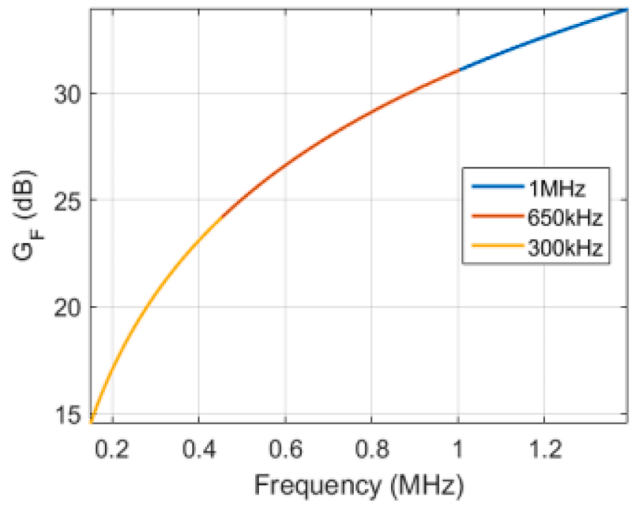

Fig. 14. Focusing gain G_F for 20 mm transducer at 25.4 mm distance.

It can be concluded that Z_{12} and Z_{21} do match within 5 %, and the only mismatch observed is for the out of band measurements, at the edges of the passband, where the SNR is low.

The electrical transfer impedance Z_{1H} and Z_{2H} measured in configurations (c) or (d) was obtained when the transducer (T_1 to get Z_{1H} and T_2 for Z_{2H}) was mounted on the parabolic mirror, and the beam was focused on the needle hydrophone tip (Fig. 13). Hydrophone tip distance from the transducer axis d was 25.4 mm, which corresponds to the focal distance of the parabolic mirror. The distance from the transducer piezo element to the hydrophone axis, d_a was 16 mm. It can be accounted for as an additional attenuation for the 16 mm distance. Diffraction over this distance was negligible, therefore this was not accounted for.

The pressure produced at the focal spot p_{RX} can be calculated from the transmitted pressure p_{TX} using linear focusing gain G_F [17,29]:

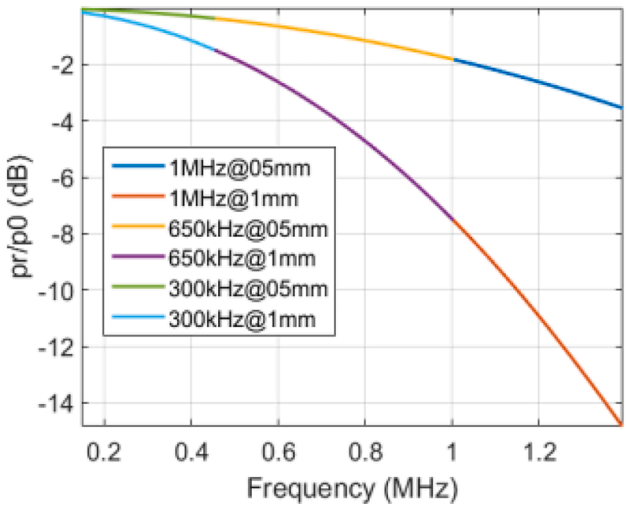

Fig. 15. Focused beam size correction $G_{BS} = p_r / p_0$ for 0.5 mm and 1 mm hydrophone.

$$p_{RX} = \frac{Af}{cd} p_{TX} = G_F p_{TX} \tag{6}$$

where f is the probing frequency.

The frequency response of the focusing gain is presented in Fig. 14.

It must be noted, that the pressure derived in (6) is the peak pressure on the beam central axis, p_0. The transducers used have a large aperture of 20 mm, and therefore the focused beam is narrow. At 0.3 MHz, the beam diameter is 1.7 mm, at 0.65 MHz it is 0.8 mm and at 1 MHz it is 0.5 mm. The normalized pressure distribution [29,30] for the focal spot can be approximated as:

$$\frac{p}{p_0} = e^{\frac{jkr^2}{2d}} \frac{2J_1\left(\frac{kar}{d}\right)}{\frac{kar}{d}} \tag{7}$$

where J_1 is the Bessel function of the first kind, $k = 2\pi f/c$ is the wave-number, r is the radial distance on the focal plane and d is the focal distance.

The average registered pressure p_r is the integral of (7) over the hydrophone sensing element's surface [31–34,39]. If the hydrophone size is larger than the beam size, the measured pressure will be underestimated (refer to Fig. 15 for p_r / p_0 over a range of frequencies). The beam size effect can be expressed as p_r / p_0 and can be addressed as a beam size correction factor $G_{BS} = p_r / p_0$. While this is negligible for the 0.3 MHz and 0.65 MHz transducers, for the 1 MHz transducers the beam size effect causes an amplitude change of −14 dB. A nominal hydrophone diameter [41,42] was used in the calculations, and the accuracy of the results can be improved by estimating the actual effective hydrophone sensitive element size [33,34,40].

Finally, the electrical transfer impedance for the transducer-hydrophone through transmission measurements can be expressed as:

$$Z_{1H} = \frac{E_{RXH1}}{I_{TX1}} = S_{P1} M_H G_{BS} G_F e^{-\alpha(d+d_a)} Z_{2H} = \frac{E_{RXH2}}{I_{TX2}} = S_{P2} M_H G_{BS} G_F e^{-\alpha(d+d_a)} \tag{8}$$

Using (2), (5) and (8), hydrophone reception sensitivity is:

$$M_{H1} = \sqrt{\frac{2G_{TT} e^{-ad} c \cdot d^2 Z_{1H} Z_{2H}}{G_{BS}^2 e^{-2\alpha(d+d_a)} A \rho f^2 Z_{12}}} M_{H2} = \sqrt{\frac{2G_{TT} e^{-ad} c \cdot d^2 Z_{1H} Z_{2H}}{G_{BS}^2 e^{-2\alpha(d+d_a)} A \rho f^2 Z_{21}}} \tag{9}$$

Reception sensitivities of the transducers T_1 and T_2 are:

$$M_1 = \sqrt{\frac{2AZ_{21}Z_{1H}}{\rho c Z_{2H} G_{TT} e^{-ad}}} M_2 = \sqrt{\frac{2AZ_{12}Z_{2H}}{\rho c Z_{1H} G_{TT} e^{-ad}}} \tag{10}$$

Transmission sensitivities of the transducers T_1 and T_2 are:

$$S_{P1} = \sqrt{\frac{\rho c Z_{12} Z_{1H}}{2AZ_{2H} G_{TT} e^{-ad}}} S_{P2} = \sqrt{\frac{\rho c Z_{21} Z_{2H}}{2AZ_{1H} G_{TT} e^{-ad}}} \tag{11}$$

The air density was always assumed 1.205 kg/m^3, and the ultrasound propagation velocity in air was estimated from the temperature measured during experiment (20–25 °C range) as [43]:

$$c = \sqrt{\frac{\gamma \Re T}{M}} = \chi \sqrt{T} \tag{12}$$

where T is the absolute temperature, γ is the adiabatic index, M is the molecular mass of the gas, and $\Re$ is the universal gas constant, χ approximately equal to 20.05 mK$^{-1/2}$s^{-1}, when M is 0.02897 kg/mol, γ is 1.4000 and $\Re$ is 8.31446261815324 J·K^{-1}·mol^{-1}.

2.4. *Effective transducer element size estimation using focused beam scan*

The effective transducer element diameter is required in order to obtain the diffraction correction and the focusing gain, using the

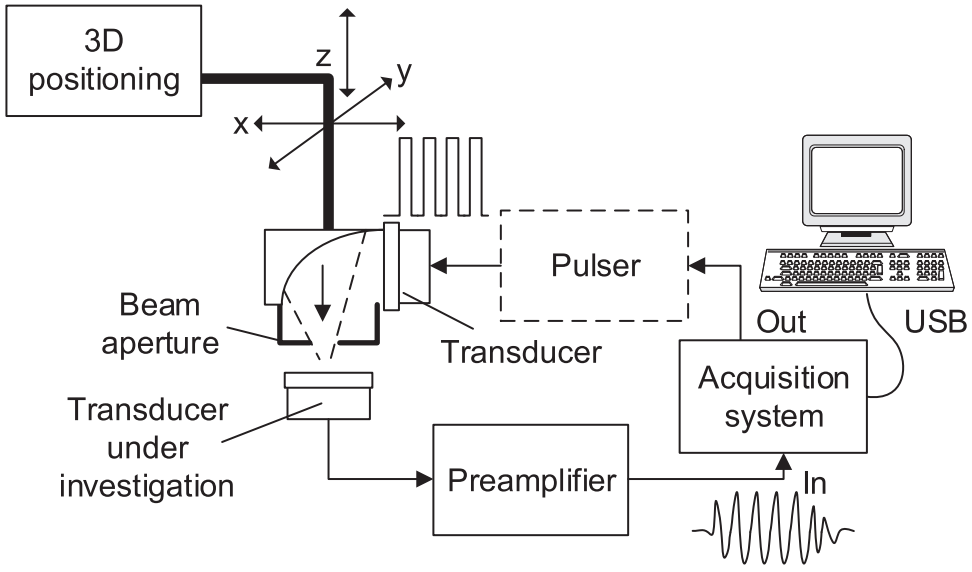

Fig. 16. Probe sensitivity map imaging setup.

parabolic off-axis mirror. The effective size of the active element can be estimated by locating the zeros along the z axis [38]. However, positioning on the symmetry axis for air-coupled transducers is problematic: the field is not homogeneous and signal peaks are very sharp.

A transducer sensitivity map [11,44] was used, in order to evaluate the effective element size. Measurement of the sensitivity map was based on the electrical output of the receiving transducer focused on the tested probe's surface. Scanning the focal spot along × and y coordinates produced the 2D sensitivity map $P_{TX}(x_{TX},y_{TX})$.

The simulated pressure distribution $p_{sim}(x_{RX},y_{RX})$ for the focal spot was calculated using the sensitivity map, $P_{TX}(x_{TX},y_{TX})$:

$$d_{TX_{n,m}} = \sqrt{\left(d^2 - \left(x^2_{TX_{n,m}} + y^2_{TX_{n,m}}\right)\right)} \tag{13}$$

$$r_{Tot_{n,m}} = \sqrt{\left(d^2_{TX_{n,m}} + \left(x_{RX} - x_{TXn,m}\right)^2 + \left(y_{RX} - y_{TXn,m}\right)^2\right)} \tag{14}$$

$$p_{sim}(x_{RX}, y_{RX}) = \sum_n \left(\sum_m \left(\frac{e^{jkr_{Tot_{n,m}}} P_{TX_{n,m}}}{r_{Tot_{n,m}}}\right)\right) \tag{15}$$

Then the normalized pressure distribution obtained by (7) was fitted to a normalized, simulated pressure distribution p_{sim} by varying the transducer radius a. The diameter, providing the best fit was considered as the effective transducer diameter.

The measurement setup for sensitivity map acquisition is presented in Fig. 16. The transducer under investigation was fixed with its active element oriented upwards, and another transducer of the same type was mounted on the off-axis parabolic mirror (as in Fig. 4). The mirror and transducer holder were attached to an x-y-z positioning stage. The × and y coordinates were used for scanning (50x50 grid with 0.5 mm step) and the z coordinate was used for focal spot placement on the transducer surface being investigated.

Transducer was excited by a half bridge topology pulser SE-TX01-02 [26], using a bipolar +/-10 V rectangular toneburst of 100 μs duration. The reception preamplifier gain was 35 dB.

2.5. Three transducers reciprocity calibration using plane wave

The transducers T_1 and T_2 can also be calibrated using a third transducer T_3 [22], instead of the hydrophone. This calibration can be used for validation purposes of the results obtained using the technique described above. Equations (10) and (11) are applied because the plane wave reciprocity is valid. The electrical transfer impedance Z_{1H} and Z_{2H} will be replaced by Z_{13} and Z_{23}, respectively:

$$Z_{13} = \frac{E_{RX31}}{I_{TX1}} Z_{23} = \frac{E_{RX32}}{I_{TX2}} \tag{16}$$

where E_{RX31} is the received voltage on the transducer T_3 output, when the transmitting transducer is T_1 and E_{RX32} is the received voltage on the transducer T_3 output, when the transmitting transducer is T_2. In this setup, the parabolic mirror focusing was not used, and all measurements were carried out at a distance of 25.4 mm (Fig. 6), so that impedances Z_{12} and Z_{21} could be used from the previous measurements.

3. Results and discussion

Two transducers of each frequency (0.3 MHz 0.65 MHz and 1 MHz), labeled as T_1 and T_2 were used together with needle hydrophones of 0.5 mm and 1 mm diameter, using the hybrid calibration technique, described in section 2.3. The result of this calibration were the hydrophone reception sensitivities M_{H1}, M_{H2} and transducer T_1 and T_2 reception sensitivities M_1, M_2 and transmission sensitivities S_1, S_2.

For validation purposes, the transducers T_1 and T_2 were also calibrated using a third transducer T_3, using three-transducer plane wave reciprocity. The result of this calibration were the transducer T_1 and T_2 reception sensitivities M_1, M_2 and transmission sensitivities S_1, S_2.

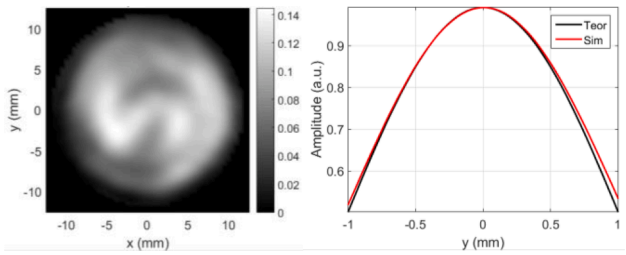

Fig. 17. Sensitivity map of the 300 kHz transducer (left) and focused beam profile obtained using this map (right).

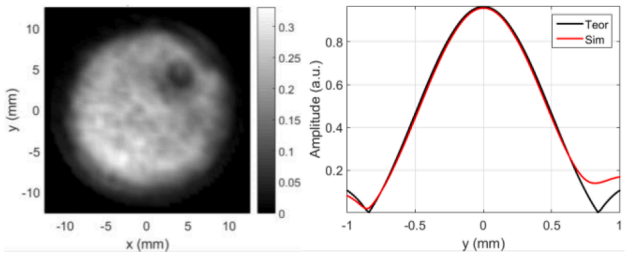

Fig. 18. Sensitivity map of the 650 kHz transducer (left) and focused beam profile obtained using this map (right).

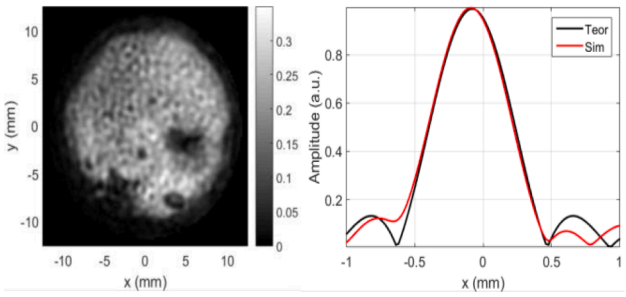

Fig. 19. Sensitivity map of the 1 MHz transducer (left) and focused beam profile obtained using this map (right).

Transducers T_1 and T_2 were also calibrated by using the substitution technique presented in [23], where a calibrated reference hydrophone was used. Since the hydrophone was calibrated for water, it was immersed in water. The signal from the air-coupled transducer was sent through the water interface. With air and water parameters available, the transmission over the air–water interface was compensated [23]. The result of this calibration were the transducer T_1 and T_2 reception sensitivities M_1, M_2 and transmission sensitivities S_1, S_2.

3.1. Effective transducer element diameter

The effective transducer element diameter, used in the calculations, was estimated from the sensitivity map, as described in section 2.4. The sensitivity map of each transducer type was measured at the center frequency. The images shown in Fig. 17 correspond to the 300 kHz center frequency transducer. Fig. 17 right is the cross-section of the simulated pressure p_{sim}/p_0 distribution (equations (13)-(15), label "Sim") comparison to fitted theoretical p/p_0 (equation (7), label "Teor").

The sensitivity is not uniform, which could be due to the thickness variation of the matching layers [35], as it is difficult to maintain precise matching layer thickness during fabrication. The effective sensitive element size was estimated to be 20.2 mm.

The images shown in Fig. 18 are for the 650 kHz center frequency transducer. The dark spot where sensitivity drops (see Fig. 18) is due to

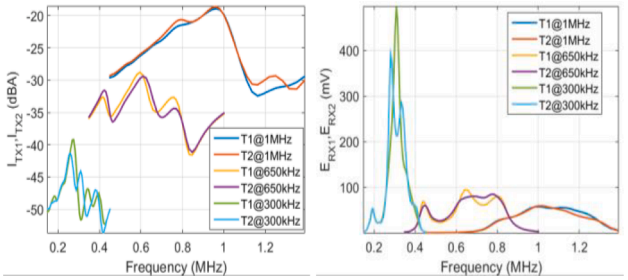

Fig. 20. Current of the transmitting transducer (left) and voltage of the receiving transducer (right) at 25.4 mm distance.

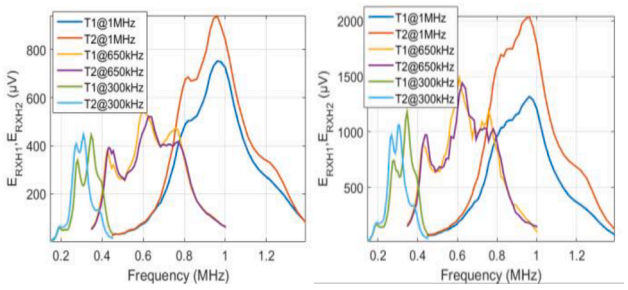

Fig. 21. Received voltage for 0.5 mm (left) and 1 mm (right) hydrophone.

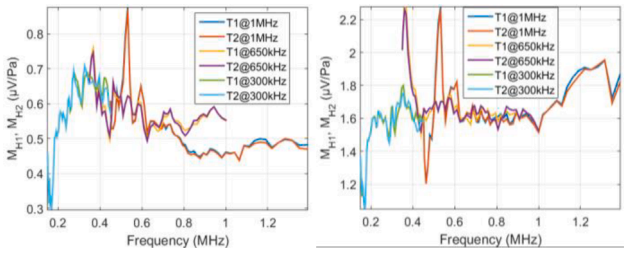

Fig. 22. Reception sensitivity for 0.5 mm (left) and 1 mm (right) hydrophone.

the soldering point of the signal electrode. The effective sensitive element size was estimated to be 18.7 mm.

The images on Fig. 19 are for the 1 MHz center frequency transducer.

At the soldering point, the sensitivity drops, which is again seen as a dark spot. Matching layer defects can be seen at the edges of the image. The effective sensitive element size was estimated to be 19.6 mm.

There was some variation of the effective element size over the range of frequencies used. Nevertheless, the values evaluated at higher than the center frequency were used for the G_{TT}, G_{da} diffraction correction factors (the focused beam size correction and focusing gain calculation). The effect of the element size on the diffraction correction factor is small, at a maximum of 1.42 dB (see Fig. 10), so that the technique can be simplified by using the nominal element size of 20 mm in the case presented.

3.2. Hydrophone sensitivity using hybrid technique

The current measured for the transmitting transducer and the corresponding received voltage in (a) and (b) configurations (transducer-transducer, refer Fig. 5) are presented in Fig. 20.

The excitation current (left), differs by more than 10 times between the transducers: for the 300 kHz transducer, it is around 10 mA max, while it is 35 mA and 110 mA for the 650 kHz and 1 MHz transducers, respectively. Meanwhile, the voltage received (right), varies in the opposite way to the current measurements: it is around 400 mV for the 300 kHz transducer, 80 mV for the 650 kHz transducer and 60 mV for

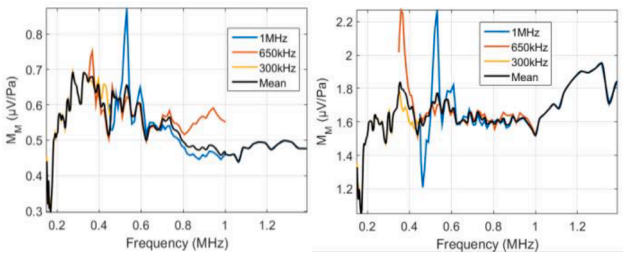

Fig. 23. Stitched hydrophone reception sensitivity for 0.5 mm (left) and 1 mm (right) hydrophone.

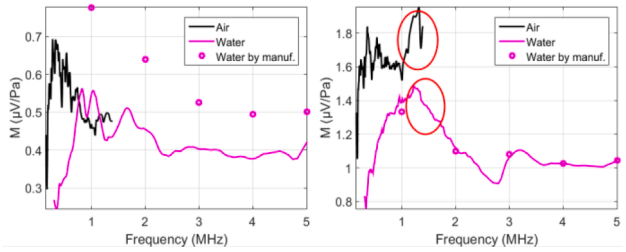

Fig. 24. Calibrated reception sensitivity in water (magenta) comparison to air (black) for 0.5 mm (left) and 1 mm (right) hydrophone (dots-manufacturer calibration certificate data). (For interpretation of the references to color in this figure legend, the reader is referred to the web version of this article.)

the 1 MHz transducer. This is expected, since the piezo element thickness is smaller for a higher center frequency, so the piezoelectric capacitance should be larger.

With the Fig. 20 and Fig. 21 data available, the hydrophone sensitivity was calculated using (9) (see results in Fig. 22).

The good match between the sensitivity of the hydrophone measurements obtained using the T_1 and T_2 transducers can serve as confirmation of the validity of the experiment setup. The mean value between results using T_1 and T_2 was taken (color lines in Fig. 23). It should be noted, that the sensitivity results obtained using different frequency range transducers overlap, but the response is not smooth. The explanation for such variability could lie in the diffraction effects and microstreaming caused by the acoustic pressure. The reception sensitivity is affected by SNR, so that at the edges of the passband of the transmitting transducer, the sensitivity is artificially increased. Results of different frequency ranges, obtained using different center frequency transducers were stitched together (black line in Fig. 23), using the received signal strength E_{RX} as a weighting factor.

In [10] it was concluded by simulations, that the hydrophone response in air and water are identical over the frequency range 50 kHz to 5 MHz. The same authors in [36] claim that the membrane

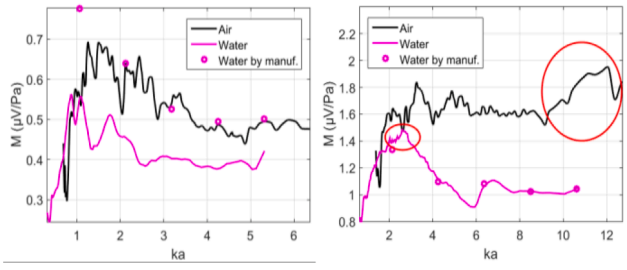

Fig. 25. Wavenumber scale plot of calibrated reception sensitivity in water (magenta) comparison to air (black) for 0.5 mm (left) and 1 mm (right) hydrophone (dots-manufacturer calibration certificate data). (For interpretation of the references to color in this figure legend, the reader is referred to the web version of this article.)

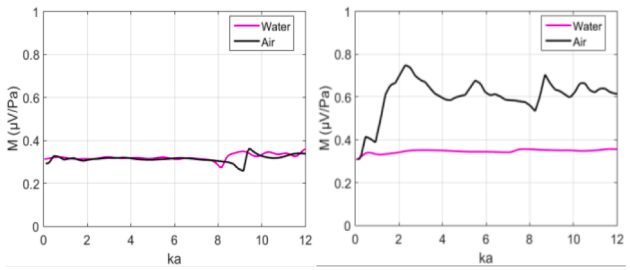

Fig. 26. Simulation results for reception sensitivity in water (magenta) and air (black) for 1 mm membrane (left) and epoxy-backed (right) 1 mm hydrophone. (For interpretation of the references to color in this figure legend, the reader is referred to the web version of this article.)

hydrophone, when calibrated in water can be applied to measurements in air without any loss of accuracy, if they are operated below their lowest resonant frequency. However, our case is different: i) the needle hydrophone has an epoxy backing, which is not the same material, as the wave propagation environment, ii) the wavelength is comparable to the transducer diameter and iii) the manufacturer's calibration certificate data is only from 1 MHz with 1 MHz steps. Therefore, a straightforward comparison to the water sensitivity results from the manufacturer's calibration certificate is not possible.

Hydrophones were calibrated in water using the standard technique: three transducers reciprocity in a free field [14]. Calibration was carried out at distance of 300 mm, using two 2 MHz transducers C2P10N-E (from Doppler Electronic Technologies Inc.). Results are presented in Fig. 24 on the frequency scale and in Fig. 25 on the radius-wavenumber product scale. It should be noted that the estimated sensitivity in water (solid magenta line) for a 0.5 mm hydrophone is lower than that indicated by the manufacturer's calibration certificate (dots). This hydrophone was used for several years extensively in various liquids, so such degradation could be expected. Therefore, the manufacturer's calibration data for the 0.5 mm hydrophone should be ignored in this case. An estimated sensitivity for the 1 mm hydrophone matches the manufacturer's calibration certificate data, except for the resonant peak at 1.2 MHz, which can also be seen on the air calibration data (red circles). One more resonance, probably related to hydrophone construction, can be noted around 3 MHz.

An important point should be noted: air-coupled calibration covers the frequency range close to low frequencies, close to the preamplifier cutoff frequency (0.1 MHz according to the manufacturer's datasheet), so that sensitivity peaking at low frequencies is reduced. Now the sensitivities in water and air can be compared, and it can be observed that the sensitivity in air is higher by 40–30 % for the 0.5 mm hydrophone, and higher by 40–60 % for the 1 mm hydrophone. This contradicts [10] and [36] claims that those should be equal. Simulation of a membrane and an epoxy-backed hydrophone was carried out using the finite element method (FEM) in the OnScale Cloud Engineering Simulation platform. The membrane hydrophone was simulated as a 1 mm diameter, 40 µm thick PVDF film. The epoxy-backed needle hydrophone was simulated as the same PVDF film attached to a 3 mm thick, 1 mm diameter epoxy filling. The parameters of the PVDF and backing material were as follows: c_{PVDF} = 2300 m/s, ρ_{PVDF} = 1780 kg/m^3, $Q_{PVDF@1MHz} = 20$ and $c_{bckg} = 2800$ m/s, $\rho_{bckg} = 2800$ kg/m^3, $\alpha_{@1MHz} = 20$ dB/MHz/cm, respectively. The simulations were run in air (at t = 20 °C, $P_{air} = 101.325$ kPa, $\rho_{air} = 1.204$ kg/m^3 and $c_{air} = 343$ m/s) and water (at t = 20 °C, $\rho_{wtr} = 1000$ kg/m^3 and $c_{wtr} = 1496$ m/s). Simulation results are presented in Fig. 26 (left: membrane, right: epoxy-backed case).

From the simulation results, it can be seen that the sensitivity in air is higher by 70 % (if resonant peaks are ignored). From these calibration and simulation results, it can be concluded, that the sensitivity in air, even when normalized by wavenumber, differs from that in water.

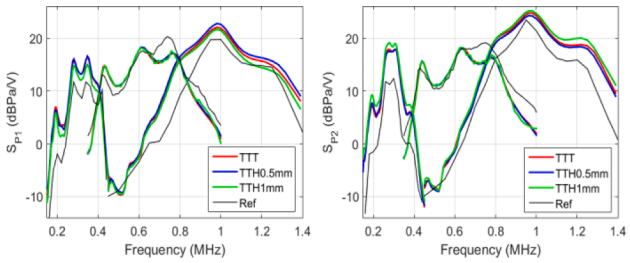

Fig. 27. Transducer plane wave transmission sensitivity for T1 (left) and T2 (right). Label "TTT" – plane wave three transducer, "TTH0.5 mm" – proposed technique using 0.5 mm hydrophone, "TTH1mm" – proposed technique using 1 mm hydrophone, "Ref" hydrophone calibration according to [23].

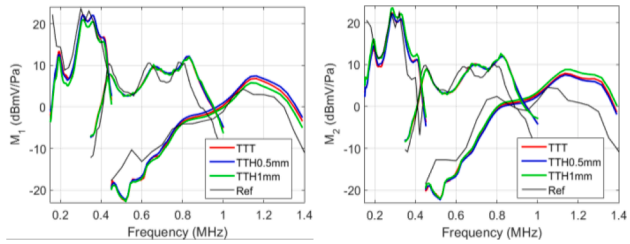

Fig. 28. Transducer reception sensitivity for T1 (left) and T2 (right). Label "TTT" – plane wave three transducer, "TTH0.5 mm" – proposed technique using 0.5 mm hydrophone, "TTH1mm" – proposed technique using 1 mm hydrophone, "Ref" - reference hydrophone calibration according to [23].

Therefore, if a hydrophone is to be used in an air-coupled configuration it should be calibrated in air.

3.3. Transducer sensitivities using three techniques

It should be noted, that the effects discussed above cancel each other out in a transducer sensitivity estimation, (10) and (11), because Z_{1H} and Z_{2H} are present in both the numerator and the denominator. Therefore, the transducer transmission sensitivity (Fig. 27) and the reception sensitivity (Fig. 28) obtained by the proposed technique, matches well to the results obtained using the plane wave [22,37] and substitution [23] calibration approaches.

It should be noted that there are some differences in the substitution technique [23] calibration results ("Ref" label in Fig. 28). The reason is that a 35 V excitation was used in the substitution technique [23], instead of the 5 V excitation voltage used in this work, so that the transducer was liable to heating, and therefore the resonance frequencies shifted towards a lower frequency value. Another reason is that a 35 V excitation is enough to generate an ultrasonic wave amplitude that will experience a significant nonlinearity in air. Some of the energy also will have leaked to higher harmonic frequencies.

There is a good match between the proposed technique results using the 0.5 mm diameter hydrophone ("TTH0.5 mm" label), the 1 mm hydrophone ("TTH1mm" label) and the plane wave, three transducer technique ("TTT" label).

4. Conclusions

A new hybrid technique involving plane wave and spherical wave reciprocity for needle hydrophones and unfocused transducers calibration in air was proposed in this paper. The proposed calibration setup is compact with a basic distance requirement of 25.4 mm, and is low cost, with a parabolic mirror costing an order of magnitude less than a focused transducer. Effects of beam diffraction, large attenuation and nonlinearity are avoided, due to the short acoustic signal path used. A convenient technique was proposed for the estimation of the effective

Table A1
Material properties used in simulation.

Material	Property		Value
Epoxy	Density	ρ_{bckg}	2800 kg/m^3
	Velocity	c_{bckg}	2800 m/s
	Attenuation @ 1 MHz	α_{bckg}	20 dB/MHz/cm
PVDF	Density	ρ_{PVDF}	1780 kg/m^3
	Velocity	c_{PVDF}	2300.62 m/s
	Quality factor @ 1 MHz	Q_{PVDF}	20
	Stiffness (constant electric field)	C_{11}	$9{\cdot}10^9$ N/m^2
		C_{12}	$6{\cdot}10^9$ N/m^2
		C_{13}	$6.5{\cdot}10^9$ N/m^2
		C_{22}	$9{\cdot}10^9$ N/m^2
		C_{23}	$6.5{\cdot}10^9$ N/m^2
		C_{33}	$8.3{\cdot}10^9$ N/m^2
		C_{44}	$2{\cdot}10^9$ N/m^2
		C_{55}	$2{\cdot}10^9$ N/m^2
		C_{66}	$1.5{\cdot}10^9$ N/m^2
	Piezoelectric stress coefficients	e15	0.2 C/m^2
		e24	0.2 C/m^2
		e31	−0.1 C/m^2
		e32	−0.1 C/m^2
		e33	0.177 C/m^2
	Dielectric constants	ε_x	9
		ε_y	9
		ε_z	8.4
Air	Density	ρ_{air}	1.204 kg/m^3
	Velocity	c_{air}	343 m/s
Water	Density	ρ_{wtr}	1000 kg/m^3
	Velocity	c_{wtr}	1496 m/s

size of the transducer active element by building a surface sensitivity map. The sensitivity map was built using the parabolic mirror's focusing. The effective element size can be estimated for every frequency, individually.

Wave amplitude estimation using the sine wave correlation technique (SWC) also extracts the phase information, which can be used for more accurate diffraction correction factor calculations, or sensitivity phase calibration.

At first glance, the proposed setup might look complex, using an off-axis mirror, employing an effective transducer diameter estimation process and requiring a precise 3D positioning system. However, the off-axis mirror is readily commercially available, and can be mounted as shown in Fig. 4, quickly and easily. The effective transducer diameter estimation step can be omitted, and the nominal diameter can be used. Furthermore, the contribution from diffraction is small, at 1.4 dB maximum, so that diffraction correction can be omitted altogether. When it comes to a precise 3D positioning system, any calibration setup has similar requirements [13,14], only at a much larger scale.

To conclude, the nonlinearity, attenuation, impedance mismatch and small hydrophone size mean that the compact setup proposed for a hydrophone calibration in air is a technically robust and cost-effective way to perform the measurements described.

Declaration of Competing Interest

The authors declare the following financial interests/personal relationships which may be considered as potential competing interests: Linas Svilainis reports financial support was provided by European Regional Development Fund.

Data availability

Data will be made available on request.

Acknowledgment

This project has received funding from European Regional Development Fund (project No. 01.2.2-LMT-K-718-03-0026) under grant agreement with the Research Council of Lithuania (LMTLT). Authors also acknowledge the help of A. Aleksandrovas and M. Varatinskas in experimental modules preparation.

Appendix A. . Material properties used in simulation

Material properties used in simulation are provided here. PVDF piezo element was loaded by propagation material (water for water case or air for air case) when membrane hydrophone was simulated. Meanwhile, for needle hydrophone case, front face was loaded PVDF piezo element was loaded by propagation material and backing used high density epoxy.

Table A1.

References

[1] T. Marhenke, S.J. Sanabria, B.R. Chintada, R. Furrer, J. Neuenschwander, O. Goksel, Acoustic field characterization of medical array transducers based on unfocused transmits and single-plane hydrophone measurements, Sensors 19 (4) (2019) 863, https://doi.org/10.3390/s19040863.
[2] R. J. Kazys, R. Sliteris, J. Sestoke, Air-Coupled Low Frequency Ultrasonic Transducers and Arrays with PMN-32%PT Piezoelectric Crystals, Sensors, vol. 17, no. 1, Jan. 2017, Art. no. 95, doi: https://doi.org/10.3390/s17010095.
[3] Non-destructive testing - Characterization and verification of ultrasonic examination equipment - Part 2: Probes, EN 12668-2:2010, 2010.
[4] Y.B. Wang, M. Sun, Y.G. Cao, J. Zhu, Application of optical interferometry in focused acoustic field measurement, J. Sound Vib. 426 (Jul. 2018) 234–243, https://doi.org/10.1016/j.jsv.2018.04.023.
[5] G. Benny, G. Hayward, Beam Profile Measurements and Simulations for Air-Coupled Ultrasonic Transducers, In Proc. IEEE IUS 1–2 (1999) 1041–1044.
[6] G. Benny, G. Hayward, R. Chapman, Beam profile measurements and simulations for ultrasonic transducers operating in air, J. Acoust. Soc. Amer. 107 (4) (Apr. 2000) 2089–2100, https://doi.org/10.1121/1.428491.
[7] G. Allevato, J. Hinrichs, M. Rutsch, J.P. Adler, A. Jager, M. Pesavento, M. Kupnik, Real-Time 3-D Imaging Using an Air-Coupled Ultrasonic Phased-Array, IEEE Trans. Ultrason. Ferroelect. Freq. Control 68 (3) (Mar. 2021) 796–806, https://doi.org/10.1109/TUFFC.2020.3005292.
[8] S.J. Sanabria, T. Marhenke, R. Furrer, J. Neuenschwander, Calculation of Volumetric Sound Field of Pulsed Air-Coupled Ultrasound Transducers Based on Single-Plane Measurements, IEEE Trans. Ultrason. Ferroelect. Freq. Control 65 (1) (Jan. 2018) 72–84, https://doi.org/10.1109/TUFFC.2017.2773619.
[9] 1/8-inch Pressure-field Microphone Type 4138, Brüel & Kjær, 2021.
[10] A. Gachagan, G. Hayward, S.P. Kelly, W. Galbraith, Characterization of air-coupled transducers, IEEE Trans. Ultrason. Ferroelect. Freq. Control 43 (4) (Jul. 1996) 678–689, https://doi.org/10.1109/58.503730.
[11] L. Svilainis, A. Chaziachmetovas, D. Kybartas, T. G. Alvarez-Arenas, Air-Coupled Ultrasonic Probe Integrity Test Using a Focused Transducer with Similar Frequency and Limited Aperture for Contrast Enhancement, Sensors, vol. 20, no. 24, Dec 2020, Art. no. 7196, doi: https://doi.org/10.3390/s20247196.
[12] P.A. Lewin, G. Lypacewicz, R. Bautista, V. Devaraju, Sensitivity of ultrasonic hydrophone probes below 1 MHz, Ultrasonics 38 (1–8) (Mar. 2000) 135–139, https://doi.org/10.1016/S0041-624X(00)00002-0.
[13] Electroacoustics - Measurement microphones - Part 3: Primary method for free-field calibration of laboratory standard microphones by the reciprocity technique, IEC 61094-3:2016, International Electrotechnical Commission, 2020.
[14] Underwater acoustics - Hydrophones - Calibration of hydrophones - Part 1: Procedures for free-field calibration of hydrophones, IEC 60565-1:2020, International Electrotechnical Commission, 2020.
[15] E. Mosland, R. Hauge, E. Storheim, M. Vestrheim, P. Lunde, and J. Kocbach, Reciprocity calibration method for ultrasonic, piezoelectric transducers in air, including finite element simulations, in Proc. SSPA, 2013, pp. 2-6.
[16] L. Gaete-Garreton, J. A. Gallego-Juárez, E. Riera, Nonlinear problems in the generation, propagation and measurement of high intensity ultrasonic waves in air, In: Proc. MA, vol. 32, 2017, Art. no. 045027, doi: 10.1121/2.0000782.
[17] A. Selfridge, P.A. Lewin, Wideband spherically focused PVDF acoustic sources for calibration of ultrasound hydrophone probes, IEEE Trans. Ultrason. Ferroelect. Freq. Control 47 (6) (Nov. 2000) 1372–1376, https://doi.org/10.1109/58.883526.
[18] W.D. Shou, S.M. Duan, P.Z. He, R.M. Xia, D.C. Qian, Calibration of a focusing transducer and miniature hydrophone as well as acoustic power measurement based on free-field reciprocity in a spherically focused wave field, IEEE Trans. Ultrason. Ferroelect. Freq. Control 53 (3) (Mar. 2006) 564–570, https://doi.org/10.1109/TUFFC.2006.1610564.
[19] D.A. Hutchins, T.J. Robertson, D.R. Billson, New designs of focused air-coupled ultrasonic transducer, Revista de Acustica 33 (2002) 3–4.
[20] T.E.G. Alvarez-Arenas, J. Camacho, C. Fritsch, Passive focusing techniques for piezoelectric air-coupled ultrasonic transducers, Ultrasonics 67 (Apr. 2016) 85–93, https://doi.org/10.1016/j.ultras.2016.01.001.
[21] T.E.G. Alvarez-Arenas, Air-Coupled Piezoelectric Transducers with Active Polypropylene Foam Matching Layers, Sensors 13 (5) (May 2013) 5996–6013, https://doi.org/10.3390/s130505996.

[22] B.D. Simmons, R.J. Urick, The Plane Wave Reciprocity Parameter and Its Application to the Calibration of Electroacoustic Transducers at Close Distances, J. Acoust. Soc. Amer. 21 (1949) 633–635, https://doi.org/10.1121/1.1906561.
[23] J. Quirce, T. G. Alvarez-Arenas, L. Svilainis, Calibration of Air-Coupled Ultrasonic Transducers, In Proc. 2021 IEEE IUS, Xi'an, China, 2021, pp. 1-4, doi: https://doi.org/10.1109/IUS52206.2021.9593482.
[24] B. Hosten, M. Castaings, Parabolic mirror and air-coupled transducer for multimodal plate wave detection, in Proc. QNDE, vol. 22, 2003, pp. 1243–1250.
[25] L. Svilainis, V. Dumbrava, S. Kitov, A. Aleksandrovas, P. Tervydis, D. Liaukonis, Electronics for Ultrasonic Imaging System, Elektron. Elektrotech. 20 (7) (2014) 51–56, https://doi.org/10.5755/j01.eee.20.7.8024.
[26] L. Svilainis, A. Chaziachmetovas, V. Dumbrava, Half bridge topology 500 V pulser for ultrasonic transducer excitation, Ultrasonics 59 (May 2015) 79–85, https://doi.org/10.1016/j.ultras.2015.01.014.
[27] L. Svilainis, A. Chaziachmetovas, T.E.G. Alvarez-Arenas, Ultrasonic Air Coupled Transducer Output Impedance Measurement Technique, Elektron. Elektrotech. 25 (1) (2019) 18–25, https://doi.org/10.5755/j01.eie.25.1.22731.
[28] T.D. Mast, F. Yu, Simplified expansions for radiation from a baffled circular piston, J. Acoust. Soc. Amer. 118 (6) (Dec. 2005) 3457–3464, https://doi.org/10.1121/1.2108997.
[29] B.G. Lucas, T.G. Muir, The field of a focusing source, J. Acoust. Soc. Amer. 72 (S41) (1982) 1289–1296, https://doi.org/10.1121/1.2019882.
[30] X. C. Chen, K.Q. Schwarz, K.J. Parker, Radiation pattern of a focused transducer: A numerically convergent solution, J. Acoust. Soc. Amer., vol. 94, no. 5, pp. 2979–2991, Nov. 1993, doi: https://doi.org/10.1121/1.407329.
[31] G. Z. Xing, P. Yang, P. C. Hu, K. H. Lam, L. B. He, Z. H. Zhang, Field characterization of steady state focused transducers using hydrophones based on Fresnel approximation, Meas. Sci. Technol., vol. 28, Jun. 2017, Art. no. 065005, doi: 10.1088/1361-6501/aa6421.
[32] K.A. Wear, Y.B. Liu, Considerations for Choosing Sensitive Element Size for Needle and Fiber-Optic Hydrophones-Part II: Experimental Validation of Spatial Averaging Model, IEEE Trans. Ultrason. Ferroelect. Freq. Control 66 (2) (Feb 2019) 340–347, https://doi.org/10.1109/TUFFC.2018.2886071.
[33] K.A. Wear, C. Baker, P. Miloro, Directivity and Frequency-Dependent Effective Sensitive Element Size of Needle Hydrophones: Predictions From Four Theoretical Forms Compared With Measurements, IEEE Trans. Ultrason. Ferroelect. Freq. Control 65 (10) (Oct. 2018) 1781–1788, https://doi.org/10.1109/TUFFC.2018.2855967.
[34] K.A. Wear, S.M. Howard, Directivity and Frequency-Dependent Effective Sensitive Element Size of a Reflectance-Based Fiber-Optic Hydrophone: Predictions From Theoretical Models Compared With Measurements, IEEE Trans. Ultrason. Ferroelect. Freq. Control 65 (12) (Dec. 2018) 2343–2348, https://doi.org/10.1109/TUFFC.2018.2872840.
[35] T.E.G. Alvarez-Arenas, Acoustic impedance matching of piezoelectric transducers to the air, IEEE Trans. Ultrason. Ferroelectr. Freq. Control 51 (5) (May 2004) 624–633, https://doi.org/10.1109/TUFFC.2004.1320834.
[36] W. Galbraith, G. Hayward, Development of a PVDF membrane hydrophone for use in air-coupled ultrasonic transducer calibration, IEEE Trans. Ultrason. Ferroelect. Freq. Control 45 (6) (Nov. 1998) 1549–1558, https://doi.org/10.1109/ULTSYM.1996.584142.
[37] R.J. Bobber, General Reciprocity Parameter, J. Acoust. Soc. 39 (1966) 680–687, https://doi.org/10.1121/1.1909941.
[38] A. Goldstein, D.R. Gandhi, W.D. O'Brien, Diffraction effects in hydrophone measurements, IEEE Trans. Ultrason. Ferroelect. Freq. Control 45 (4) (1998) 972–979.
[39] E.G. Radulescu, P.A. Lewin, A. Goldstein, A. Nowicki, Hydrophone spatial averaging corrections from 1 to 40 MHz, IEEE Trans. Ultrason. Ferroelect. Freq. Control 48 (6) (Nov. 2001) 1575–1580, https://doi.org/10.1109/58.971709.
[40] Ultrasonics - Hydrophones - Part 3: Properties of hydrophones for ultrasonic fields. IEC 62127-3:2022. International Electrotechnical Commission, 2020.
[41] 5 mm needle hydrophone (NH1000). Technical data sheet. Precision acoustics.
[42] 0 mm needle hydrophone (NH1000). Technical data sheet. Precision acoustics.
[43] S.L. Garrett. Understanding Acoustics: An Experimentalist's View of Sound and Vibration. 2nd ed. 2020.
[44] L Svilainis, A Chaziachmetovas, A Aleksandrovas, D Kybartas, TG Alvarez-Arenas, Air Coupled Probe Integrity Test Using Same Type Probe on Parabolic Mirror, In Proc. IEEE IUS, 2022. DOI10.1109/IUS54386.2022.9958231.